Int. J. Electrochem. Sci., 11 **(2016)** 8530 – 8545, doi: 10.20964/2016.10.18

International Journal of
ELECTROCHEMICAL
SCIENCE
www.electrochemsci.org

Electrochemical Impedance Spectroscopy Characteristic of Ti-6Al-4V Alloy with and Without Welding under the Different Load Model

Yan Liu[1], *Shawei Tang*[1], *Guangyi Liu*[1,2], *Yue Sun*[1], *Jin Hu*[1,*]

[1] School of Materials Science and Engineering, Harbin Institute of Technology, Harbin 150001, China
[2] State Key Laboratory for Marine Corrosion and Protection, Luoyang Ship Material Research Institute (LSMRI), Qingdao 266101, China
[*]E-mail: hujin@hit.edu.cn

Received: 31 May 2016 / *Accepted:* 29 July 2016 / *Published:* 6 September 2016

Electrochemical impedance spectroscopy (EIS) measurements are performed on a Ti-6Al-4V alloy with and without welding. EIS measurements are always performed simultaneously on two identical specimens: one stressed with a slow strain rate tensile test or a constant load test and one free of stress test. A similar electrochemical characterization is exhibited on the alloys with and without welding during exposure in a LiCl-methanol solution. However, their corrosion mechanisms in the corrosion media are completely different. The difference in the surface states of the welded and non-welded alloy is responsible to the change of the corrosion mechanism. The welded alloy exhibit high susceptibility to corrosion and stress corrosion cracking. The applied stress promotes the corrosion process.

Keywords: Ti-6Al-4V alloy; Laser beam welding; Electrochemical impedance spectroscopy; SSRT

1. INTRODUCTION

Titanium and its alloys have been widely employed in aeronautical, nuclear, chemical, medical and civil applications due to the excellent comprehensive mechanical properties and chemical compatibility [1-3]. Furthermore, titanium and its alloys have high corrosion resistant due to the formation of TiO_2 on its surface [4]. TiO_2 is a stable and dense layer, which acts as a protective barrier to continued metallic oxidation [5]. However, some external condition, such as abnormal cyclic loads, acidic environments and their conjoint effects, can rupture the protective oxide film and result in permanent breakdown of the oxide film. Consequently, the underlying metal may exposure to corrosive mediums [6]. There are numerous studies about stress corrosion cracking of titanium and its

alloys. Tsai *et al.* [7] reported the stress corrosion cracking susceptibility of Ti–6Al–4V alloy in Lewis-neutral aluminium chloride–1-ethyl-3-methylimidazolium chloride ionic liquid. Trasatti *et al.* [8] found that water contents affected the stress corrosion cracking susceptibility of pure titanium in *n*-propanol and *iso*-propanol solutions. Pustode *et al*. [9] obtained a critical temperature to occur stress corrosion cracking for Ti-6A1-2Sn-4Zr-2Mo-0.1Si alloy in hot salt. It has been shown that titanium and its alloys are susceptible to stress corrosion cracking in a series variety of application environments.

Due to the requirement of working conditions of titanium alloys, welding technology have been widely developed [10-12]. The welding process is considered to have a harmful influence on corrosion behavior of welded titanium alloys. Because of a phase transformation (martensitic transformation) can happen in the fusion zone or in the heat-affected-zone. This change of crystaline structure can affect the corrosion properties of titanium. Han *et al.* [13] investigated the corrosion behavior of scanning electron beam welded Ti–6Al–4V alloy in acid $CuSO_4$ solution. The author found that the fusion zone had lower corrosion potential and higher corrosion current densities compared with the base metal. Similar conclusions about corrosion behavior of gas tungsten arc welding Ti–6Al–4V alloy in Ringer solution were reported by Heidarbeigy *et al*. [14] and Karimzadeh *et al*. [15]. The authors found that the base metal possessed higher corrosion resistance compared with the fusion zone, which was indicated by the more noble corrosion potential and lower corrosion current density. As mentioned above, fusion zone was considered as a particularly sensitive zone to corrosion due to the special structure in comparison to the base metal. However, thus far, there has been very few research conducted on the difference of the corrosion characteristic and corrosion mechanism between the welded and non-welded titanium alloy under applied stress in corrosion environments, especially in an environments which can cause the stress corrosion cracking of titanium alloy. Titanium alloy shows excellent corrosion resistance in aqueous solution, but can suffer from corrosion in anhydrous organic medium such as methanol solution under the presence of applied stress, particularly the existence of chloride as LiCl [8].

It is generally known that electrochemical impedance spectroscopy is considered to be an effective tool to study the electrochemical corrosion characteristics and can provide information about process of electrodes reaction, which has been widely used in various materials [16-18]. It has been reported that electrochemical impedance spectroscopy used in combination with slow strain rate tensile and constant load test to study the corrosion behavior in common structural materials such as steel and aluminum [19-21], but there has been few report on the titanium alloy. Particularly, the relevant aspects of research on the titanium alloy weldment are still very scanty. In this study, we investigate the electrochemical corrosion behavior (EIS characteristic) of welded and non-welded Ti-6Al-4V alloy in a LiCl-methanol solution under the different load model: slow strain rate tensile test, constant load test and one free of stress test for comparison. The effect of stress on corrosion resistance of welded and non-welded Ti-6Al-4V alloy has been discussed. To make sure the quality of the EIS data, Kramers-Kronig transformations are used to validate the experimental data.

2. EXPERIMENTAL

2.1 Materials and welding

Commercially available mill-annealed Ti-6A1-4V alloy sheet with dimensions of 240mm×50mm×1mm is prepared for laser welding in this work. The chemical composition of the alloy is shown in Table 1.

Table 1. Chemical compositions (wt.%) of Ti–6A1–4V alloy.

Element	Ti	Al	V	Fe	C	O	H	N
Content	Balance	5.9	4.0	0.08	0.02	0.1	0.002	0.3

All joints are welded by using a Rofin-DC030 3kW laser beam system. The welding process parameters are listed in Table 2. Surface oxides and contamination are removed from the surfaces of the prepared samples by mechanically brushed and cleaned with acetone prior to the welding. Due to the strong reaction at high temperature between ambient gases and Ti–6A1–4V alloy, pure argon is utilized for avoiding oxidation of the fusion zone and heat affected zone during the welding process. The area of the welding zone on the welded plate is 4.8 cm^2.

Table 2. Parameters of laser beam welding.

Power (W)	Frequency (Hz)	Welding speed（m/min）	Argon pressure (MPa)
800	35	1	0.12

2.2. Slow strain rate tensile and constant load test

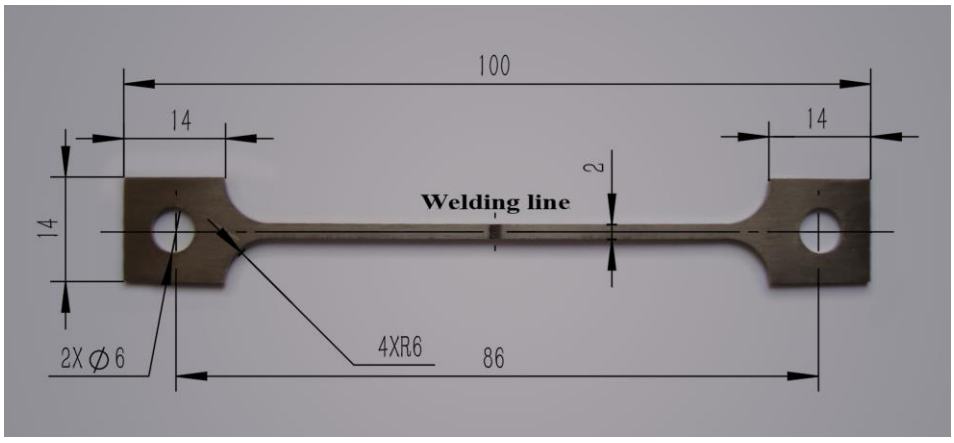

Figure 1. Dimensions of the tensile specimen, mm.

Slow strain rate tensile (SSRT) test is conducted in air and 0.1 mol/L LiCl-methanol solution, respectively. The strain rate of the SSRT is 3×10^{-7}/s [22,23]. Fig. 1 exhibits the dimensions of the tensile specimen, the area of the welding zone is 0.12 cm^2. Constant load test is conducted under various external stresses, which is 0,400 (50% $\sigma_{0.2}$) and 800 MPa (100% $\sigma_{0.2}$) [20].

2.3. Electrochemical measurements

Electrochemical impedance spectroscopy (EIS) and potentiodynamic polarization tests are performed through Gamry Reference 3000 electrochemical measurement system in the LiCl-methanol solution. A silver/silver chloride/methanol reference electrode is employed in this study. Test specimens are used as a working electrode and graphite is used as a counter electrode. The potential scan rate is 5mV/s during potentiodynamic polarization tests. EIS measurements are performed couple with the SSRT test and the constant load test. During the SSRT process, EIS measurements are done every 2 h regularly from the beginning up to the failure of the tensile specimens. An AC potential perturbation with amplitude of 10 mV is applied on the tensile specimen at open circuit potential and the range of measuring frequency is from 100 kHz to 10 mHz.

2.4. Microstructure and fracture surface analysis

The workpieces are cross sectioned transverse to the welding direction. The cross-sections are prepared by grinding, polishing and etching with Kroll's reagent. Microstructure analysis is carried out using metallographic microscope (Olympus PMG2).

The fractured features of the tensile specimens are observed through Hitachi S-3000N scanning electron microscope.

3. RESULTS AND DISCUSSION

3.1 Microstructures of Ti-6Al-4V alloy with and without welding

A typical microstructure of the studied samples is shown in Fig. 2. There are two different phases exist in Ti-6Al-4V alloy (Fig. 2a). One is the dark β phase (body-centered cubic structure), the other is the bright equiaxed α phase (hexagonal close-packed structure). The β phase distribute at the α phase boundaries.

Fig. 2b shows the microstructure of the fusion zone in the welded sample, which consist of the fine acicular α′ martensite solidification structure (supersaturated nonequilibrium hexagonal phase) with different crystallographic orientations. In comparison to the fusion zone, the heat affected zone shows some different and more complex microstructures. The heat affected zone locate between the fusion zone and the base metal can be classified into two parts depend on the different microstructures, the near-heat affected zone (close to the fusion zone) and the far-heat affected zone (close to the base metal). The microstructure of the near-heat affected zone is almost the same as that of the fusion zone,

the acicular α′ martensite phase is observed in the zone (Fig. 2c). Hence, the near-heat affected zone can be identified as the fully transformed region. The acicular α′ martensite phase, original α phase and original β phase are observed in the far-heat affected zone, as shown in Fig. 2d. The presence of the remaining original α phase and original β phase reveal the incomplete transformation from the β phase to the α phase, thus, the far-heat affected zone can be considered to be the partially transformed region. The microstructure of laser welding Ti–6A1–4V alloy was observed by many researches, the similar microstructure such as fusion zone and heat affected zone have been analyzed well [10-12].

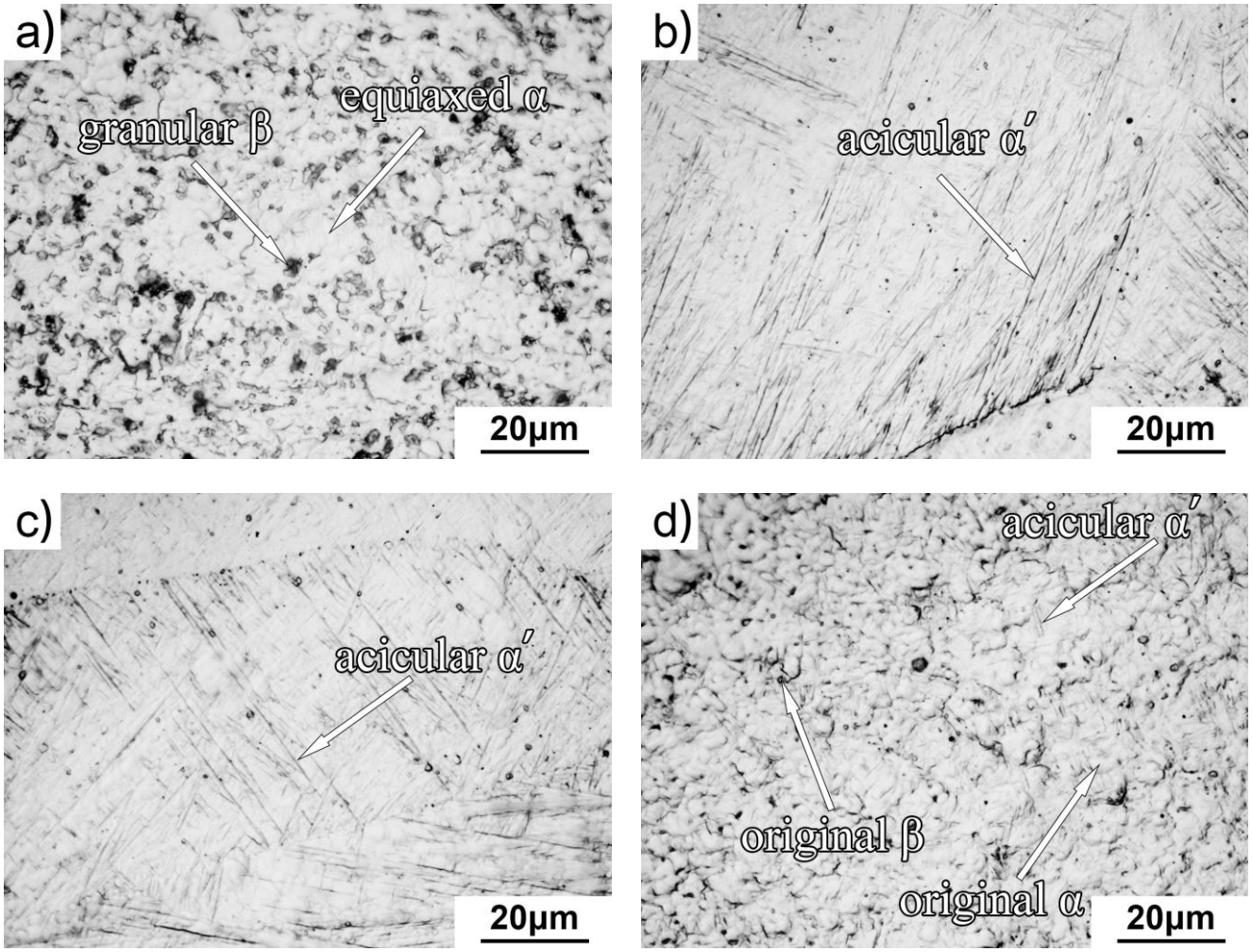

Figure 2. Microstructure of the laser beam welding Ti-6Al-4V alloy (1000X): (a) base metal; (b) fusion zone; (c) near-heat affected zone; (d) far-heat affected zone.

3.2 Corrosion susceptibility of the welded sample in the corrosion media

As mention above in this paper, the welding process can deteriorate the corrosion resistance of titanium alloy. In order to realize the corrosion behavior of the welded sample, the polarization curves of the samples with and without welding are detected as shown in Fig. 3. It can be found that the polarization behaviors are different for the two specimens. For the non-welded sample, the corrosion

potential is -0.162 V and the anodic current density increase slowly with the potential, which cause a passive region in the anodic polarization curve of the non-welded sample and breakdown potential with value of 0.036 V.

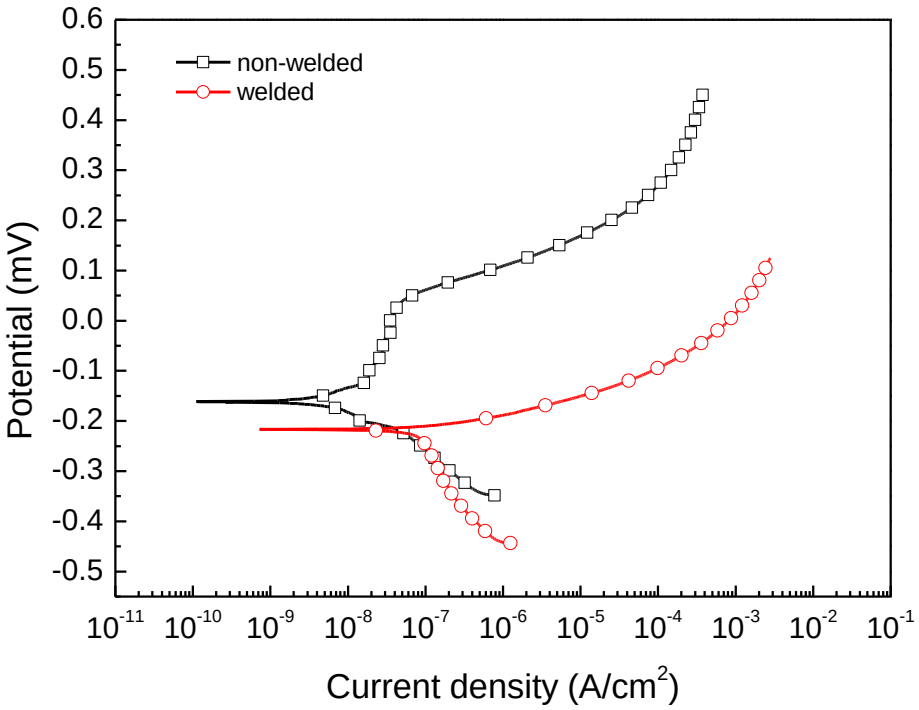

Figure 3. Polarization curves of the Ti-6Al-4V alloy with and without welding in the solution.

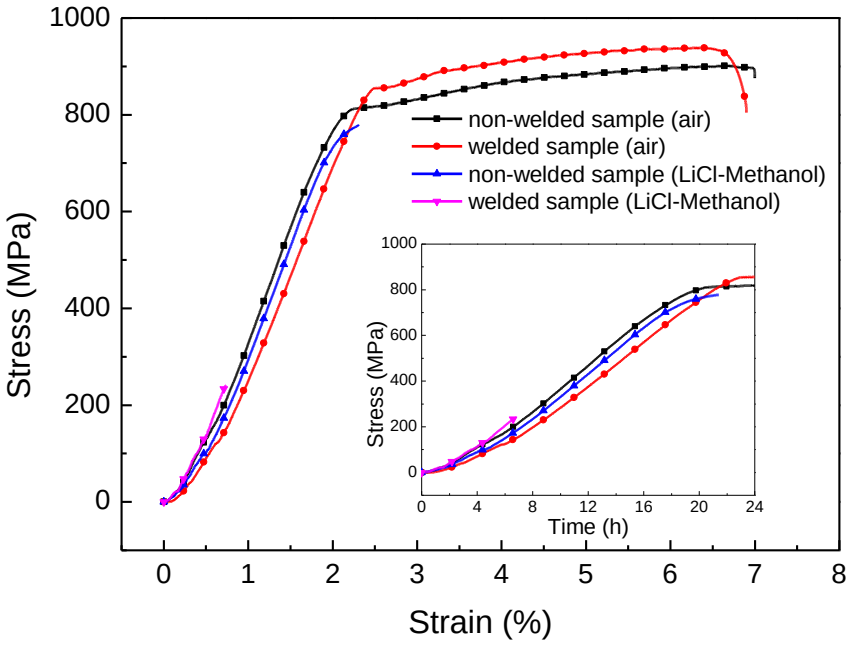

Figure 4. Stress-strain curves of the Ti-6Al-4V alloy with and without welding during the SSRT process.

The similar passivation phenomenons can also be found in other polarization curves measured in HCl-methanol and LiCl-propanol solutions [8,23]. Ti-6Al-4V alloy exhibit resistance to local corrosion because the alloy is well protected by its native oxide film [24-26]. For the welded sample, the corrosion potential is -0.217 V and the anodic current density increase rapidly with the potential. A lower pitting potential exist in the anodic polarization curve. The poor corrosion resistance is observed due to the presence of the welding seam, which is consistent with many researches [13-15].

The slow strain rate test is applied to evaluate the susceptibility to stress corrosion cracking [27,28]. Fig. 4 exhibits the stress-strain curves of the samples with and without welding during the SSRT process. For comparison, the samples are also tested in air under the same test conditions. For the non-weld samples, the ultimate tensile strength and elongation to fracture is low and the fracture time is short in the LiCl-methanol solution. This indicates that Ti-6Al-4V alloy has SCC susceptibility in the corrosion media. Moreover, it can be clearly found that the ultimate tensile strength and elongation to fracture of the welded sample in the LiCl-methanol solution are terribly low and the fracture time is much short. It is without question, the SCC susceptibility of the welded Ti-6Al-4V alloy in LiCl-methanol solution is very high.

The fractograph morphologies of the welded samples are exhibited in Fig. 5. All of the specimens fracture in the fusion zone. There are numerous dimples on the fractograph of the specimen tested in air (Fig. 5a), indicating that a good capability of plastic deformation exists in the sample. Transgranular cleavage fracture is found on the fractograph of the specimen tested in LiCl-methanol solution (Fig. 5b), which results from the brittle fracture. These phenomena are consistent with the Fig. 4, which further show high susceptibility to SCC of the welded sample in LiCl-methanol solution. This is in agreement with the previous researches on titanium alloy. The similar fractograph morphologies were observed by. Gao *et al.* [10] and Yin *et al.* [23].

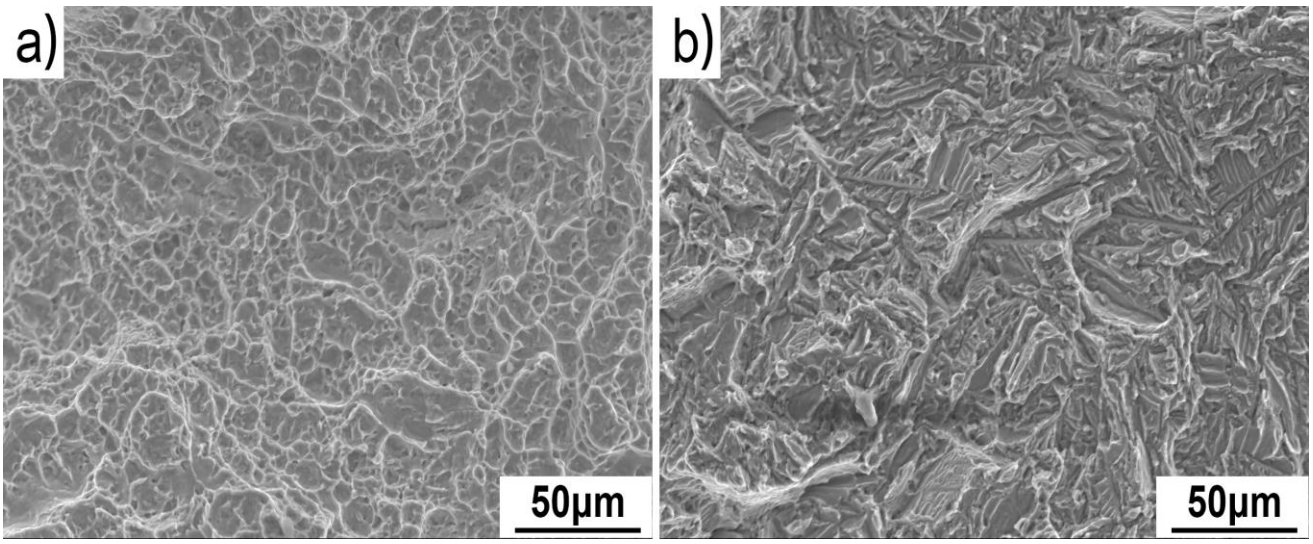

Figure 5. Fractograph morphologies of the welded Ti-6Al-4V alloy after SSRT test (500X): (a) tested in air; (b) tested in solution.

3.3 Electrochemical impedance spectroscopy analysis

Electrochemical impedance spectroscopy technique provides effective description of electrochemical characteristics of corrosion behavior [29-32]. In order to investigate the electrochemical characteristic of the welded specimen, the electrochemical impedance spectra are performed simultaneously on two identical samples: one with a SSRT or a constant load, the other one with a free stress.

3.3.1 EIS with the SSRT test

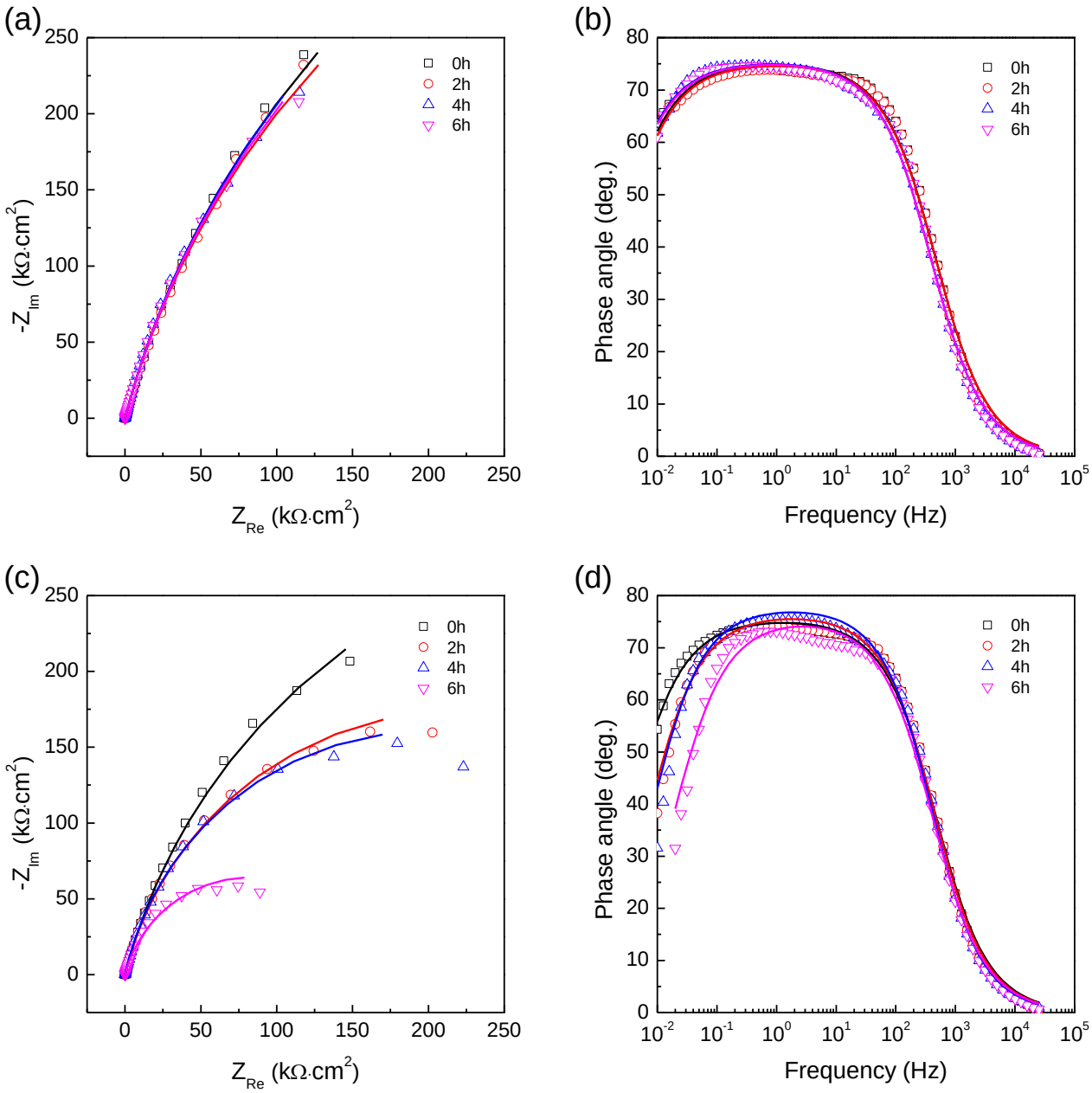

Figure 6. Evolution of the electrochemical impedance spectra of the welded Ti-6Al-4V alloy (symbols are experimental data and solid lines are fitting data): (a) Nyquist plots of the stress free sample; (b) Bode plots of the stress free sample; (c) Nyquist plots of the stressed sample; (d) Bode plots of the stressed sample.

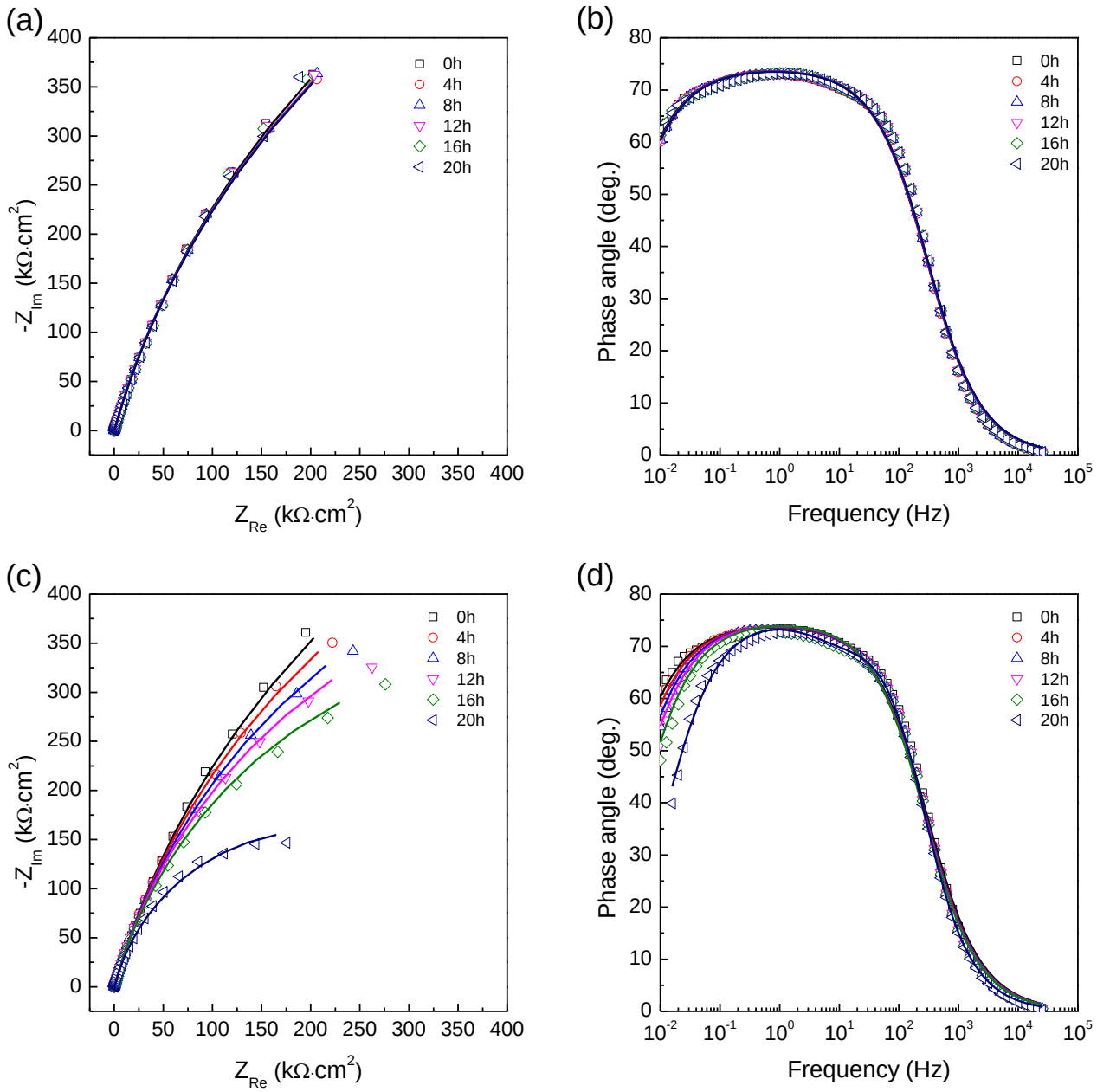

Figure 7. Evolution of the electrochemical impedance spectra of the non-welded Ti-6Al-4V alloy (symbols are experimental data and solid lines are fitting data): (a) Nyquist plots of the stress free sample; (b) Bode plots of the stress free sample; (c) Nyquist plots of the stressed sample; (d) Bode plots of the stressed sample.

Fig. 6 and Fig. 7 exhibit the evolution of the electrochemical impedance spectra of the specimens with and without welding, respectively.

For the welded sample, the Nyquist plots show a capacitance loop and the Bode plots clearly present a time constant in the measurement process. Either the radius of the capacitance loop or the phase angle of the stress free sample is almost no change (Fig. 6a and 6b), and yet the radius of the capacitance loop and the phase angle of the stressed sample decrease continuously (Fig. 6c and 6d) with the increasing of the immersion time. Similar phenomena exist in the non-welded sample. That is, the Nyquist plots and Bode plots of the stress free sample are almost no change during the immersion

process (Fig. 7a and 7b), and yet the radius of the capacitance loop and the phase angle of the stress sample decrease continuously during the SSRT process (Fig. 7c and 7d).

From Fig. 6 and Fig. 7, it can be found that when the samples are free of stress, either the non-welded or welded samples, their Nyquist plots show a capacitance loop in the immersion process and the radiuses of the capacitance loops are almost no change. When the samples stressed with the SSRT, the Nyquist plots also show a capacitance loop during the SSRT process. The radius of the capacitance loop decrease continuously with the increasing of the immersion time. The fracture times of the non-welded and welded samples are 20 h and 6 h, respectively. Particularly, when the immersion time is more than 20 h, the Bode plots for the non-welded sample stressed with the SSRT contain two time constants, which relate to the breakdown of the oxide film exist on the sample surface [33,34].

The EIS of stressed and stress free samples can be fitted by the equivalent circuit in Fig. 8, and a good correspondence between the fitted (solid lines as shown in Fig. 6 and Fig. 7) and measured spectra is obtained. In this work, R_s is the solution resistance, Q_f and R_f mean the capacitance and resistance for the TiO_2 film, Q_{dl} and R_{ct} mean the capacitance and resistance for the substrate metal. These equivalent circuits have been widely used to describe the corrosion behavior of titanium alloy in various corrosive medium [35-37]. Fig. 9 presents the fitting values of the elements.

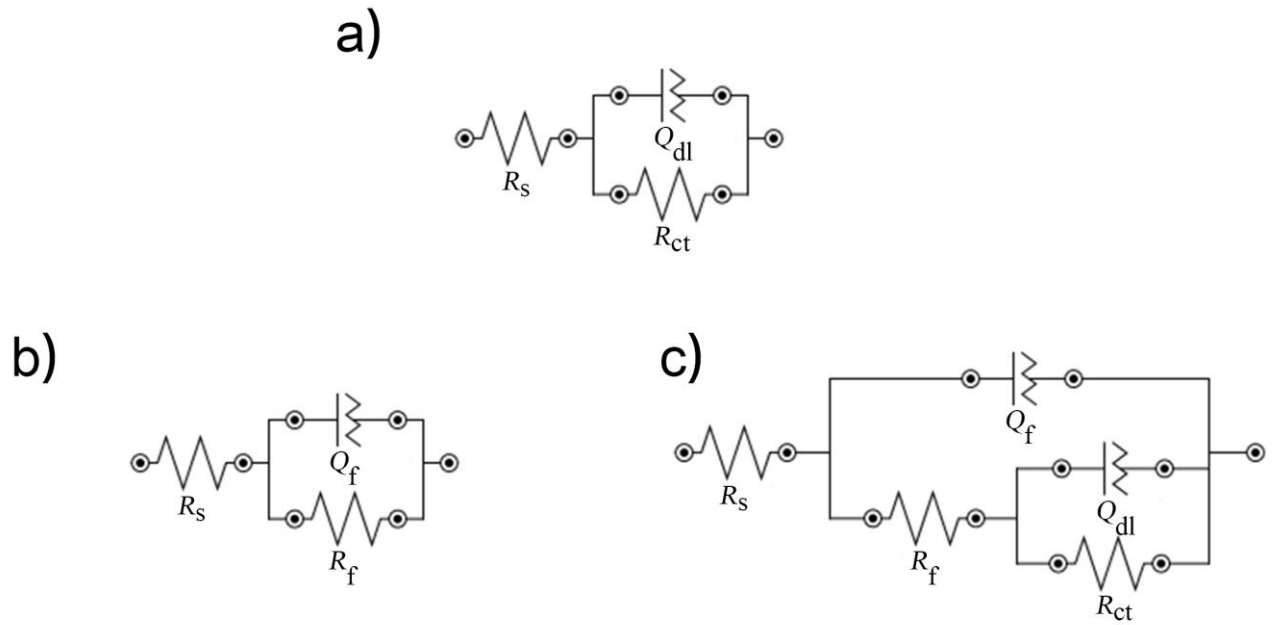

Figure 8. Equivalent circuit models for the impedance spectra of the welded and non-welded samples during different periods: (a) for the stressed and stress free welded sample; (b) for the non-welded sample with free of stress, 0 h-16 h for the stressed non-welded sample; (c) 20 h for the stressed non-welded sample.

The obvious differences are observed in the charge transfer resistance of the welded samples and oxide film resistance of the non-welded samples. To the welded sample (as shown in Fig. 9a), there is little change in the R_{ct} value for the stress free sample, and yet the R_{ct} continuously decline during the SSRT test. In addition, the R_{ct} value of the stress free sample is always higher than that of

the stressed sample. The charge transfer resistance is proportional to the corrosion resistance of the specimens [38,39]. The continual stressing promotes the susceptibility of the weld sample to occur corrosion, resulting in the R_{ct} decreasing.

To the non-welded sample (as shown in Fig. 9b), the oxide film resistance of the stress free sample almost maintain a certain lever. However, the R_f continuously decrease before 16 h which is followed by a rapid decrease during the SSRT test.

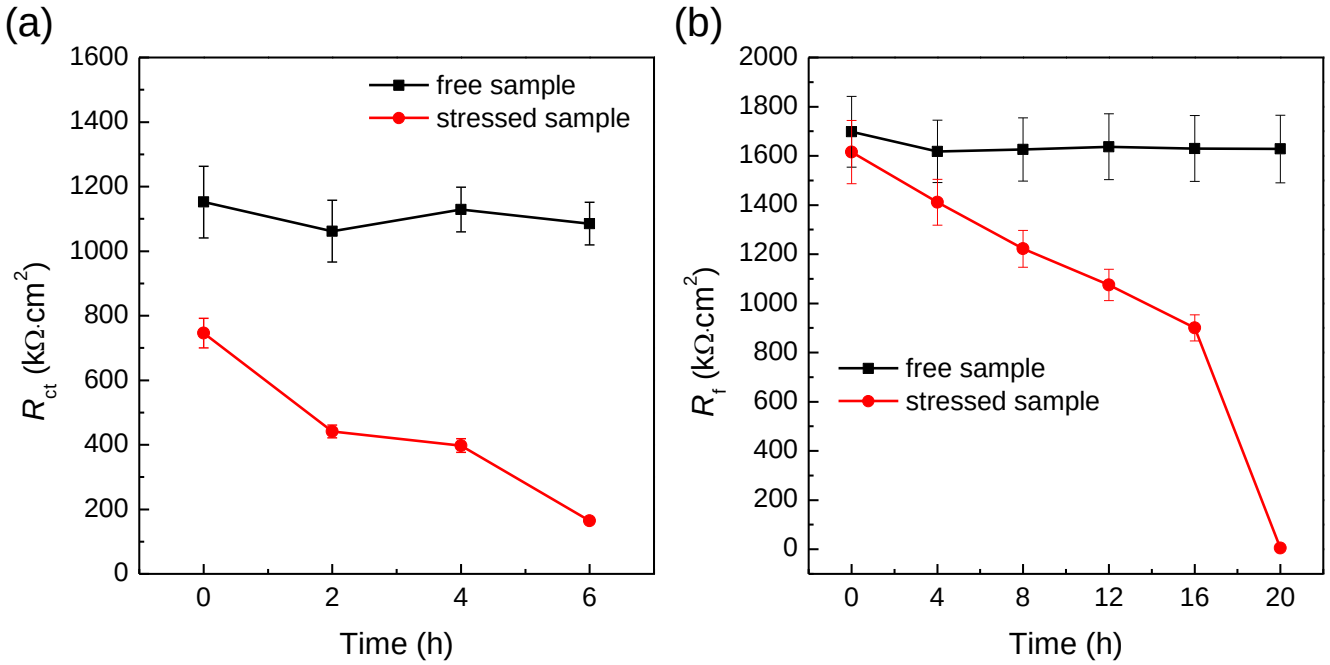

Figure 9. EIS fitting values of the elements: (a) R_{ct} (b) R_f.

A natural oxide film can form on Ti-6Al-4V alloy. The oxide film can protect the stress free sample in the corrosion media, thus R_f maintain no change during the immersion process [40-42]. However, the oxide film is destroyed gradually during the SSRT process, therefore the oxide film resistance decrease gradually. The oxide film will lose its resistance as soon as it is broke, the R_f will decrease rapidly. In this case, the corrosion of Ti-6Al-4V alloy is accompanied by appearance of a new time constant in the low frequency region (as shown in Fig. 7d), which is in agreement with the Ref. [43,44].

3.3.2 EIS with a constant load

EIS measurements are performed on the samples with and without welding, and these samples are stressed with the different constant load, the Nyquist plots are shown in Fig. 10. There is only one time constant over the whole frequency in the spectra, corresponding to the electrochemical double layer (for the welded sample) and oxide film resistance (for the non-welded sample), respectively. The radius of the capacitance loop of the two samples decreases with the increase in the applied load.

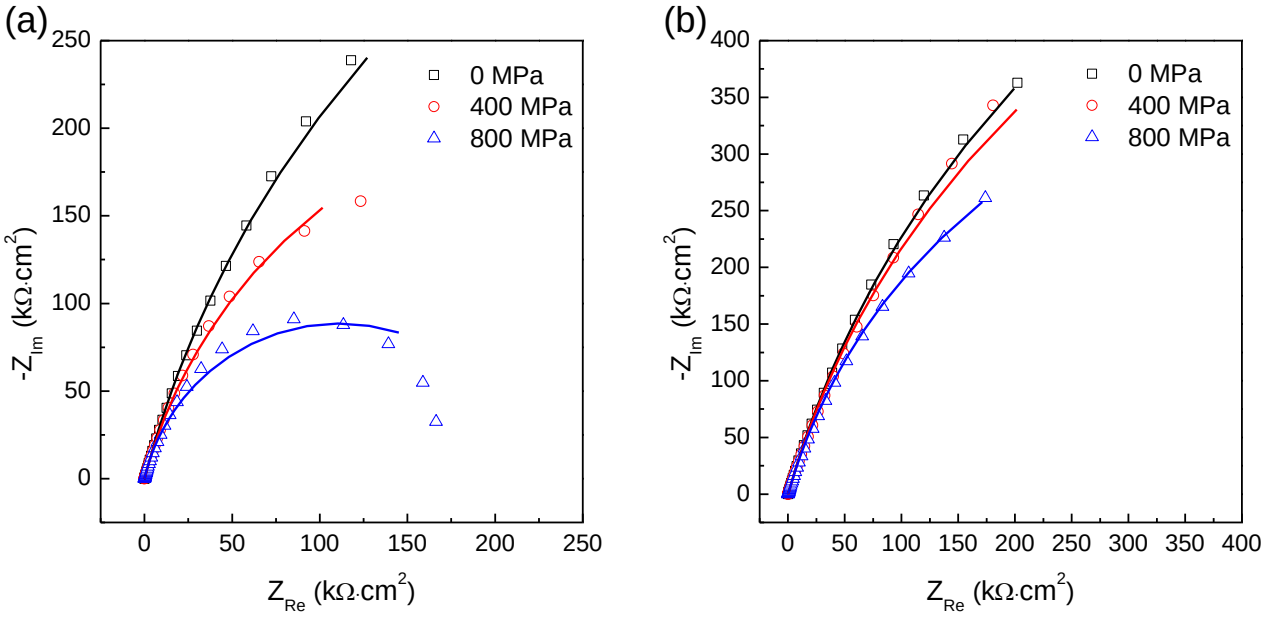

Figure 10. Electrochemical impedance spectra of the welded and non-welded Ti-6Al-4V alloy tested under the constant loads (symbols are experimental data and solid lines are fitting data): (a) welded sample; (b) non-welded sample.

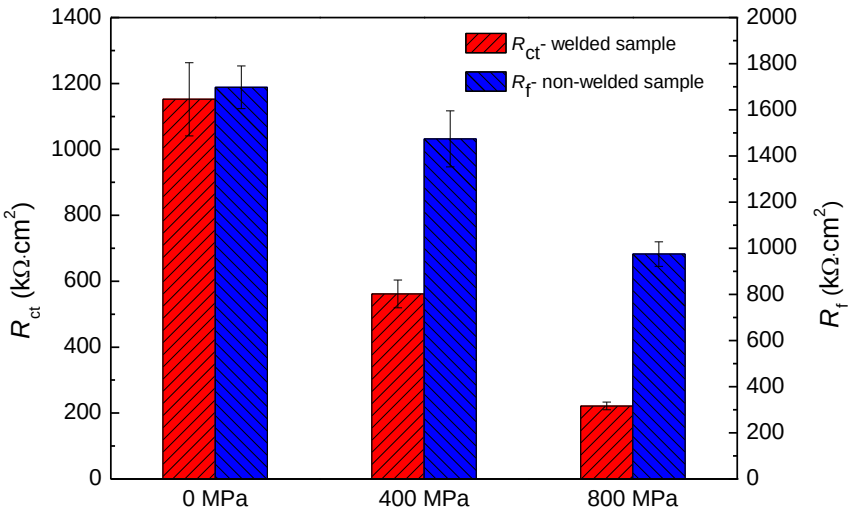

Figure 11. Fitting values of the elements under the constant load: (a) R_{ct} (b) R_f.

The EIS of the welded and non-welded samples can also be fitted by the equivalent circuit in Fig. 8a and Fig. 8b. The fitting values of the elements are presented in Fig. 11. From Fig. 11, it can be found that the R_{ct} and R_f obviously decrease with the increasing of the applied stress.

From the fitting results of the non-welded samples, it is shown that the load stress reduce the oxide film resistance, which indicates that the integrality of the oxide film is destroyed. The higher the load stress is, the greater the damage of the oxide film is, and the lower the corrosion resistance of the sample will be [43,44].

For the welded samples, it is difficult to form an intact oxide film on the sample surface. Once the sample is immersed into the corrosion solution, it will immediately be subjected to corrosion. The applied stress increase the susceptibility of the welded sample to corrosion, R_{ct} of the welded sample become lower under the higher load stress, resulting in the more poor corrosion resistance appearing in the stressed sample. This can be explained by Eq. (1).

According to the Gutman′s theory of mechanical-electrochemical interactions [45], the applied stress can affect the electrochemical activity which is expressed by the change of the equilibrium electrochemical potential according to the following formula:

$$\Delta\varphi_0 = -\frac{\Delta P V_m}{zF} \quad (1)$$

Where ΔP is the applied stress (Pa), V_m is the molar volume of the electrode material (m^3/mol), z is the charge number and F is the Faraday′ constant (96485C/mol). As shown in the formula, the applied stress (ΔP>0) in this work can reduce the electrochemical potential, and lead to the higher electrochemical activity and the stronger corrosion tendency of the stressed specimen compare with the stress free specimen. To the stressed specimens, the load on the specimens gradually increase and lead to the increasing electrochemical activity, therefore, the corrosion resistance decreases gradually during the SSRT and the constant loading process. However, the electrochemical activity of the stress free samples is low because the samples are only subjected to the erosion of the corrosion solution. Therefore, whether the R_{ct} or the R_f are high.

3.4 Kramers-Kronig transformation

The application of Kramers-Kronig transformation is considered to be effective for verifying the quality of the experimental electrochemical impendence data [19,46]. Fig. 12 shows the Kramers-Kronig transformations of the experimental data. As can be seen, the Kramers-Kronig transformations excellently fit the experimental data over the tested frequency range.

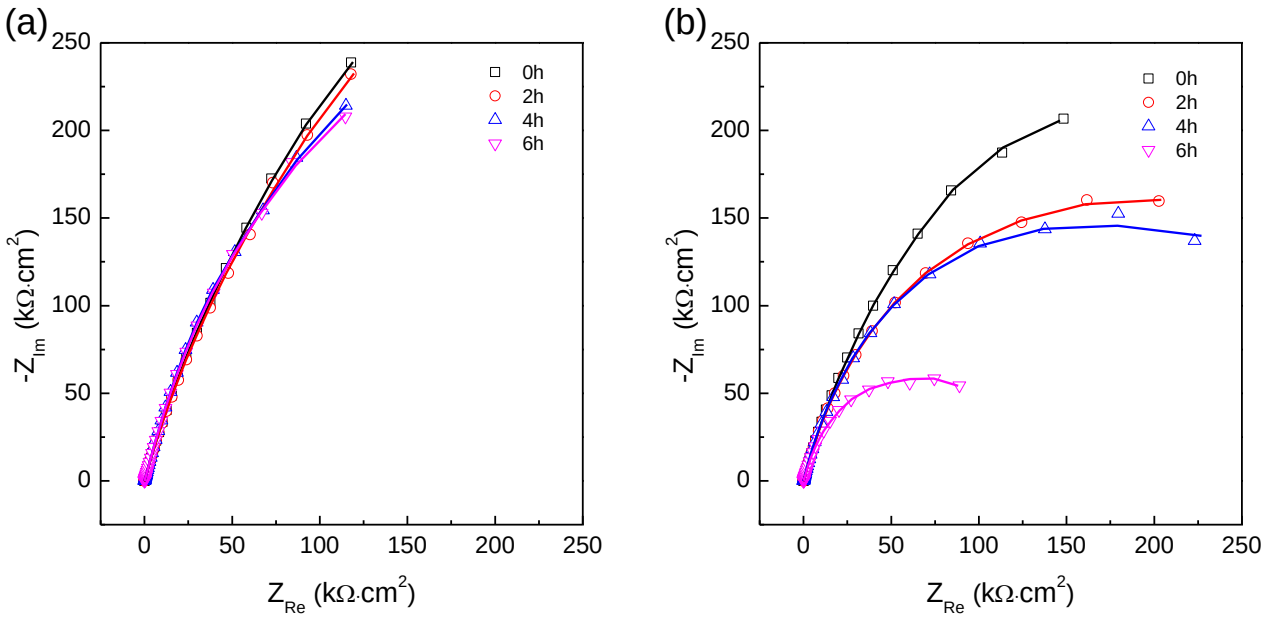

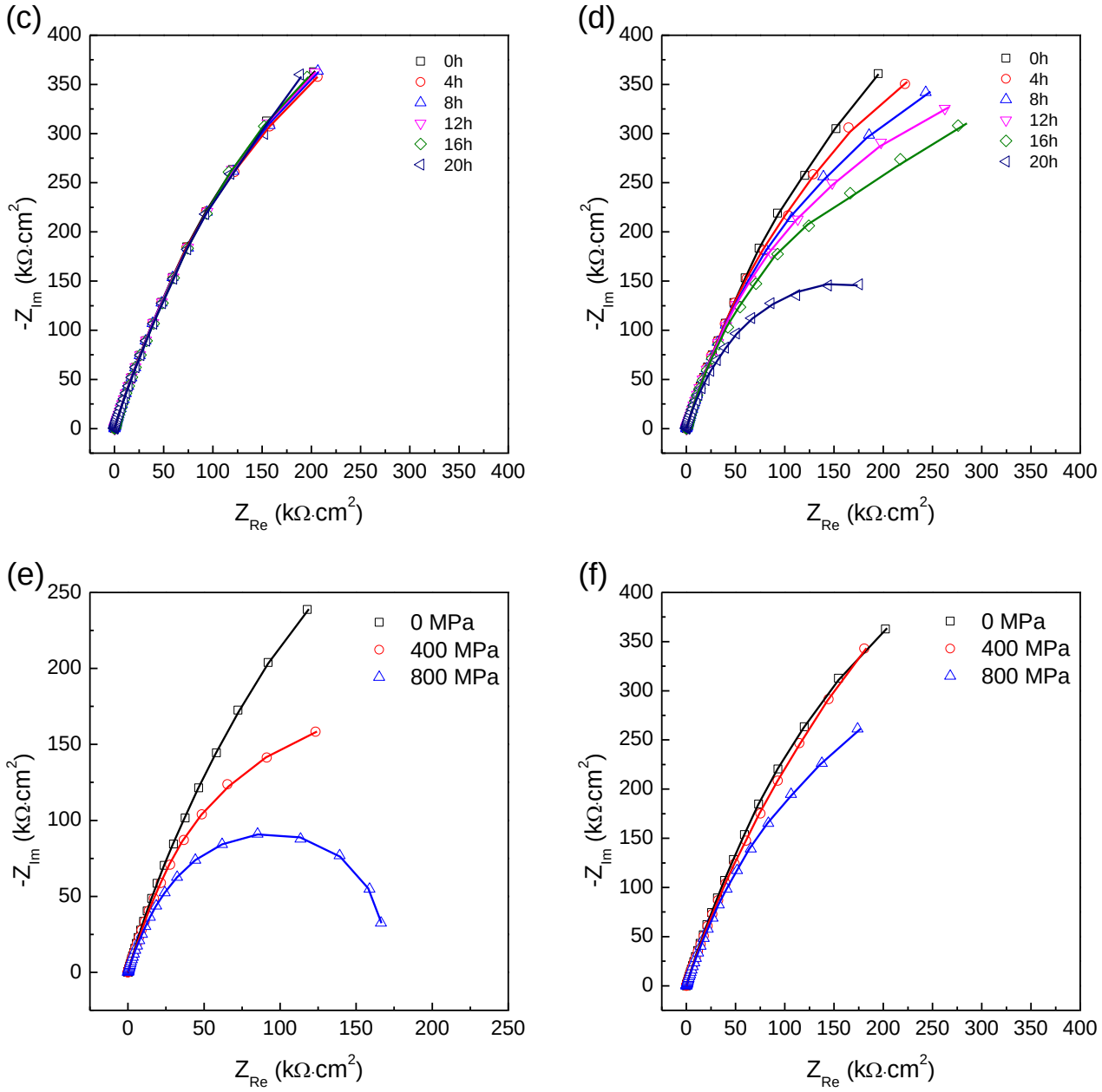

Figure 12. Kramers-Kronig transformation of the electrochemical impedance spectra (symbols are experimental data and solid lines are fitting data): (a) welded sample with free of stress; (b) welded sample under the SSRT; (c) non-welded sample with free of stress; (d) non-welded sample under the SSRT; (e) welded sample under the constant loads; (f) non-welded sample under the constant loads.

4. CONCLUSIONS

A study about the electrochemical impedance spectroscopy of Ti-6Al-4V alloy with and without welding in LiCl-methanol solution under different load mode is carried out and the EIS characteristic of the studied samples are discussed. The conclusions are addressed as follows:

(1) Ti-6Al-4V alloy has high corrosion resistance and low susceptibility to stress corrosion cracking in the LiCl-methanol solution. The welded Ti-6Al-4V alloy has high susceptibility to corrosion and stress corrosion cracking in the same solution.

(2) Electrochemical measurements for the SSRT experiments and the constant load experiments show that, in the immersion process, the general shapes of the EIS curves for both welded sample and non-welded sample are similar. However, their corrosion mechanisms in the corrosion media are completely different.

(3) All of the samples exhibit one capacitance loop in the Nyquist plots and a time constant can be observed in the Bode plots during the experimental process. Two time constants appear on the Nyquist plots at 20 h for the non-welded sample during the SSRT testing, which is relate to the destruction and dissolution of the native oxide layer.

(4) For the non-welded sample, the applied stress reduces the integrality of the oxide film and cause the decline of the oxide film resistance during the immersion process. The welding process significantly change the corrosion resistance of Ti-6Al-4V alloy, the applied stress play a critical role in corrosion behavior of the welded sample. The electrochemical activity of the welded samples is enhanced by the applied stress. There are significant difference of the charge-transfer resistance between the stress free specimens and the stressed specimens. A lower charge-transfer resistance presents in the stressed specimens which implies a stronger tendency to corrosion.

(5) Kramers Kronig Transformations show a good quality of impedance data measured in the present paper.

References

1. J. Liu, X. L. Gao, L. J. Zhang, J. X. Zhang, *Engineering Fracture Mechanics*, 117 (2014) 84-93.
2. X. L. Gao, J. Liu, L. J. Zhang, J. X. Zhang, *Materials Characterization*, 93 (2014) 136-149.
3. X. Cao, M. Jahazi, *Optics and Lasers in Engineering*, 47 (2009) 1231-1241.
4. S.A. Fadl-allah, Q. Mohsen, *Applied Surface Science*, 256 (2010) 5849-5855.
5. D. Mareci, R. Chelariu, A. Cailean, F. Brinza, G. Bolat, D.M. Gordin, *Transactions of Nonferrous Metals Society of China*, 25 (2015) 345-352.
6. A.L. Pilchak, A.H. Young, J.C. Williams, *Corrosion Science*, 52 (2010) 3287-3296.
7. W. T. Tsai, C. L. Lin, S. J. Pan, *Corrosion Science*, 76 (2013) 494-497.
8. S.P. Trasatti, E. Sivieri, *Materials Chemistry and Physics*, 83 (2004) 367-372.
9. M.D. Pustode, V.S. Raja, N. Paulose, *Corrosion Science*, 82 (2014) 191-196.
10. X. L. Gao, L. J. Zhang, J. Liu, J. X. Zhang, *Materials Science and Engineering: A*, 559 (2013) 14-21.
11. H. Liu, K. Nakata, N. Yamamoto, *Journal of Materials Science*, 47 (2012) 1460-1470.
12. P. Q. Xu, L. Li, C. Zhang, *Materials Characterization*, 87 (2014) 179-185.
13. Z. Han, H. Zhao, X. Y. Chen, H. C. Lin, *Materials Science and Engineering: A*, 277 (2000) 38-45.
14. M. Heidarbeigy, F. Karimzadeh, A. Saatchi, *Materials Letters*, 62 (2008) 1575-1578.
15. F. Karimzadeh, M. Heidarbeigy, A. Saatchi, *Journal of Materials Processing Technology*, 206 (2008) 388-394.
16. M. Atapour, M.H. Fathi, M. Shamanian, *Materials and Corrosion*, 63 (2012) 134-139.
17. K. Hagihara, M. Okubo, M. Yamasaki, T. Nakano, *Corrosion Science*, (2016).
18. Y. Wang, W. Zhao, H. Ai, X. Zhou, T. Zhang, *Corrosion Science*, 53 (2011) 2761-2766.
19. A.A. Oskuie, T. Shahrabi, A. Shahriari, E. Saebnoori, *Corrosion Science*, 61 (2012) 111-122.

20. M. Sun, K. Xiao, C. Dong, X. Li, P. Zhong, *Corrosion Science*, 89 (2014) 137-145.
21. S. Sunada, N. Nunomura, *Archives of Metallurgy and Materials*, 58 (2013).
22. Z. Qin, X. Pang, Y. Yan, L. Qiao, H.T. Tran, A.A. Volinsky, *Corrosion Science*, 78 (2014) 287-292.
23. J.O. Yin, Y.S. Wu, J. Lu, B.F. Ding, L. Zhang, B. Cao, *Rare metal materials and engineering*, 32 (2003) 436-439.
24. E. McCafferty, J.P. Wightman, *Applied Surface Science*, 143 (1999) 92–100.
25. N. Casillas, S.R. Snyder, W.H. Smyrl, H.S. White, *Journal of Physical Chemistry*, 95 (1991) 7002-7007
26. C.J. Boxley, H.S. White, C.E. Gardner, J.V. Macpherson, *Journal of Physical Chemistry*, 107 (2003) 9677-9680.
27. C.J. Alonso1, J.G. Rodriguez1, J. Chavarin1, J.G. Nava, *International Journal of Electrochemical Science*, 10 (2015) 5249-5263.
28. H. Zhang, X.D. Wang, R.L. Jia, J. Hou, W.M. Guo, *International Journal of Electrochemical Science*, 8 (2013) 1262-1273.
29. G.A. Zhang, Y.F. Cheng, *Electrochimica Acta*, 55 (2009) 316-324.
30. G.A. Zhang, Y.F. Cheng, *Corrosion Science*, 52 (2010) 960-968.
31. G.A. Zhang, Y.F. Cheng, *Corrosion Science*, 51 (2009) 1714-1724.
32. X. Tang, Y.F. Cheng, *Electrochimica Acta*, 54 (2009) 1499-1505.
33. F.E.T. Heakal, K.A. Awad, *International Journal of Electrochemical Science*, 6 (2011) 6483-6502.
34. Q. Qu, Y. He, L. Li, M. Yang, B. Lai, Y. Chen, *International Journal of Electrochemical Science*, 10 (2015) 7453-7464.
35. J.E.G. Gonza´lez, J.C. M. Rosca, *Journal of Electroanalytical Chemistry*, 471 (1999) 109–115.
36. C.H. Zhang, W. Song, F.B. Li, X. Zhao, Y.M. Wang, G.Z. Xiao, *International Journal of Electrochemical Science*, 10 (2015) 9167-9178.
37. R. Ittah, I. Malka, I. Bar, D. Itzhak, *International Journal of Electrochemical Science*, 10 (2015) 1326-1342.
38. L.Y. Xu, Y.F. Cheng, *Corrosion Science*, 59 (2012) 103-109.
39. Y.X. Wang, W.M. Zhao , H. Ai, X.G. Zhou, T.M. Zhang, *Corrosion Science*, 53 (2011) 2761-2766.
40. R.M. A. Shahba, W.A. Ghannem, A.E.E. Shenawy, A.S.I. Ahmed, S.M. Tantawy, *International Journal of Electrochemical Science*, 9 (2014) 633-643.
41. C.G.N. Dino, R.G.B. Margulis, M.A.N. Flores, M.V.O. Carmona, S.D. Torre, J.G.G. Rodriguez, J.G.C. Nava, A.M. Villafañe, *International Journal of Electrochemical Science*, 7 (2012) 4250-4260.
42. C.G.N. Dino, C.L. Meléndez, R.G.B. Margulis, M.A.N. Flores, J.G.C. Nava, S.D. Torre, J.G.G. Rodriguez, A.M. Villafañe, *International Journal of Electrochemical Science*, 7 (2012) 2389-2402.
43. R.Ittah, E. Amsellem, D. Itzhak, *International Journal of Electrochemical Science*, 9 (2014) 633-643.
44. Z. Qin, X.L. Pang, L.J. Qiao, *International Journal of Electrochemical Science*, 9 (2014) 4352-4360.
45. E.M. Gutman, Mechanochemistry and Corrosion Prevention of Metals, Science Publication, Peking (1989).
46. R.W. Bosch, *Corrosion Science*, 47 (2005) 125-143.